

# Thin film growth of the Weyl semimetal NbAs

Wilson Yanez,<sup>1</sup> Yu-Sheng Huang,<sup>1</sup> Supriya Ghosh,<sup>2</sup> Saurav Islam,<sup>1</sup> Emma Steinebronn,<sup>1</sup> Anthony Richardella,<sup>1</sup> K. Andre Mkhoyan,<sup>2</sup> and Nitin Samarth<sup>1,\*</sup>

<sup>1</sup>*Department of Physics, Pennsylvania State University,  
University Park, Pennsylvania 16802, USA*

<sup>2</sup>*Department of Chemical Engineering and Materials Science,  
University of Minnesota, Minneapolis, Minnesota 55455, USA*

(Dated: May 2, 2023)

## Abstract

We report the synthesis and characterization of thin films of the Weyl semimetal NbAs grown on GaAs (100) and GaAs (111)B substrates. By choosing the appropriate substrate, we can stabilize the growth of NbAs in the (001) and (100) directions. We combine x-ray characterization with high-angle annular dark field scanning transmission electron microscopy to understand both the macroscopic and microscopic structure of the NbAs thin films. We show that these films are textured with domains that are tens of nanometers in size and that, on a macroscopic scale, are mostly aligned to a single crystalline direction. Finally, we describe electrical transport measurements that reveal similar behavior in films grown in both crystalline directions, namely carrier densities of  $\sim 10^{21} - 10^{22}$

The TX class (T=Ta/Nb X=As/P) of transition metal monopnictides is a promising quantum materials platform for studying topological phenomena of contemporary interest because the bulk band structure corresponds to that of a topological Weyl semimetal [1–4]. Broken inversion symmetry in this class of materials leads to Weyl nodes with different chiralities; when projected onto the surface of the crystal, these nodes are connected by topological surface states (Fermi arcs) [1, 2, 4–6]. Interesting physical phenomena observed in these canonical Weyl semimetals include the chiral anomaly in charge transport, transport in the quantum limit under high magnetic fields, phase transitions between different topological states, strong intrinsic spin Hall effect, and symmetry-induced non-trivial spin-orbit torque [5, 7–10]. Most prior studies of this family of topological semimetals have used bulk single crystal samples; while these are of high structural quality, thin film samples are more desirable if these Weyl semimetals are to become useful for technological applications in microelectronics or optoelectronics. This provides a strong motivation for heterointegration of TX thin films with materials compatible with semiconductor processing; thin film growth would also enable the modulation of the band structure by controlling strain in the crystal [3, 11].

In this study, we develop the synthesis of NbAs thin films on a GaAs substrate using molecular beam epitaxy (MBE). We show that the growth of NbAs along different crystalline directions can be stabilized by judicious choice of the substrate direction. We then use x-ray diffraction to understand the macroscopic structure of the films, in addition to characterization using atomic force microscopy and electrical transport measurements. Finally, we use

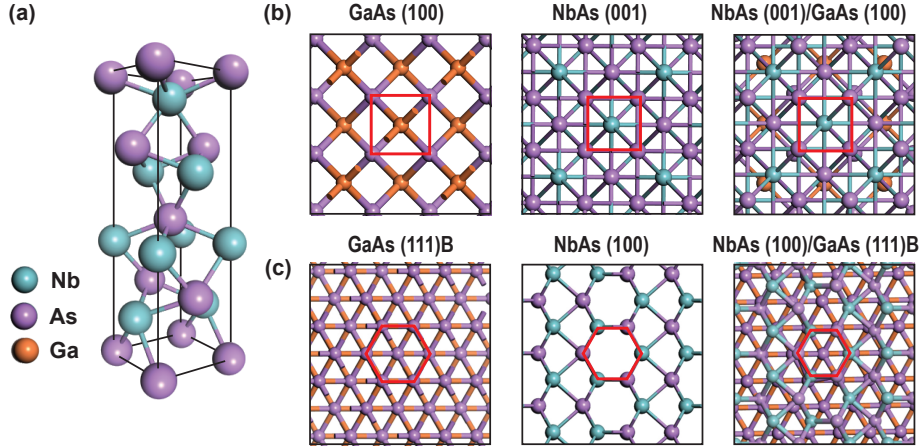


FIG. 1. (a) Crystal structure of NbAs. (b) Top view of GaAs (100), NbAs (001) and NbAs (001) on top of GaAs (100). (c) Top view of GaAs (111)B, NbAs (100) and NbAs (100) on top of GaAs (111)B. We show the square and hexagonal symmetry and lattice mismatch between the films and the substrates.

high-angle annular dark-field scanning transmission electron microscopy (HAADF-STEM) to show that our films are textured with domains that show a clear crystal structure and are tens of nanometers in size.

We first discuss the choice of substrate for the growth of NbAs thin films. NbAs is a transition metal monopnictide that has 12 pairs of Weyl nodes in its band structure [1, 4, 11]. It is a member of the  $I4_1md$  space group and crystallizes in a body-centered tetragonal structure (Fig. 1(a)) with a lattice constant of  $a = 0.345$  nm and  $c = 1.168$  nm [1, 2, 11]. It is difficult to find an adequate substrate with a lattice constant in this range [12]. Based on previous reports of MBE growth of this family of semimetals [5, 13–15], we tried using different III-V semiconductors (GaAs, GaP and InAs) as our substrates. Among these, the best results were achieved in GaAs which had a lower lattice mismatch than InAs and, unlike GaP, had the right surface chemistry to promote NbAs growth. In this paper, we focus on studying NbAs films grown on GaAs; further information about characterization of NbAs on other substrates can be found in the supplemental material [16].

An analysis of the crystal structure of NbAs suggests that the growth of NbAs (001) can be stabilized by using GaAs (100) as a substrate (Fig. 1(b)): here, the lattice mismatch is 16% along the  $\langle 110 \rangle$  and 18% along the  $\langle 100 \rangle$  GaAs directions. Although this is a very large

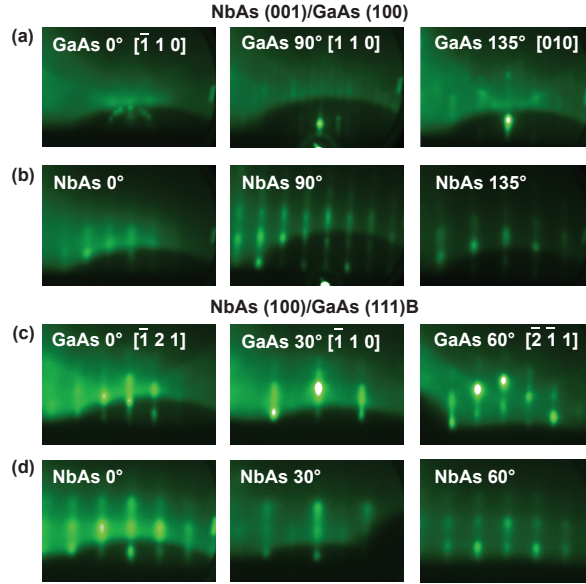


FIG. 2. RHEED pattern of: (a) GaAs (100) substrate along the  $[\bar{1}10]$ ,  $[110]$  and  $[010]$  directions. (b) NbAs (001) thin film along the same directions as (a), (c) GaAs (111)B substrate along the  $[\bar{1}21]$ ,  $[\bar{1}10]$  and  $[\bar{2}\bar{1}1]$  directions, and (d) NbAs (100) thin film along the same directions as (c).

lattice mismatch within the context of epitaxial growth, it is within range to allow NbAs to grow with a  $45^\circ$  rotation with respect to the  $\langle 100 \rangle$  GaAs direction. NbAs (100) has a similar relationship with GaAs(111) as a substrate: Fig. 1(c) shows that if we superimpose both lattices, the NbAs atoms roughly align with the hexagonal structure of GaAs(111) with a 17% mismatch on each side.

We carry out the synthesis of the NbAs films in a VEECO 930 MBE chamber while monitoring the growth using reflection high energy electron diffraction (RHEED) at 12 keV (Fig. 2). We desorb the native oxide on an epitaxially semi-insulating GaAs substrate and then grow 30 nm of GaAs at a thermocouple temperature of  $720^\circ\text{C}$  using Ga (5N) and As (5N) sources evaporated from standard effusion cells. The As:Ga beam equivalent pressure ratio is  $\sim 14$  (as measured using an ion gauge). After this, we cool down the substrate to a thermocouple temperature of  $400^\circ\text{C}$  in the presence of As flux. At this point, we observed a RHEED pattern showing a  $2 \times 4$  surface reconstruction for GaAs (100) (Fig. 2(a)) and a C6 symmetry for GaAs (111)B (Fig. 2(c)). We then increase the substrate temperature to  $700\text{-}750^\circ\text{C}$  (measured by a thermocouple in the substrate manipulator) and simultaneously deposit As and Nb (the latter from a SPECS EBE-4 4 pocket e-beam evaporator), obtaining

the RHEED pattern shown in Figs. 2(b) and 2(d). In the case of NbAs grown on GaAs (100) (Fig. 2(b)), the RHEED pattern is different in the  $[110]$  and  $[1\bar{1}0]$  directions. This follows the C2 symmetry of the GaAs substrate in the  $2 \times 4$  reconstruction. In the case of NbAs grown on GaAs (111)B (Fig. 2(c) and 2(d)), the NbAs RHEED pattern is the same in the GaAs  $[1\bar{2}1]$  and  $[2\bar{1}\bar{1}]$  crystal directions which are  $60^\circ$  apart. This indicates a C6 symmetry in the NbAs thin film due to twinning during growth.

To characterize our films on a macroscopic scale, we use x-ray diffraction. First, we perform a coupled  $2\theta - \omega$  scan on NbAs grown on GaAs (100) (Fig. 3(a)) and detect the presence of diffraction peaks from NbAs (001). Second, we perform a similar scan on NbAs grown on GaAs (111)B (Fig. 3(b)) and detect the presence of NbAs (100). We emphasize that these different crystalline planes are not equivalent due to the tetragonal crystal structure of NbAs (Fig. 1). To quantify the degree of crystallinity in our films, we perform a rocking curve ( $\omega$  scan) around the NbAs peaks and obtain a full width half maximum (FWHM) of  $1.3^\circ$  for NbAs (001) and  $2.1^\circ$  for NbAs (100). To understand the planar structure of our films, we measure a pole figure around the NbAs  $\{112\}$  direction. We observe the presence of two different sets of peaks corresponding to GaAs  $K\alpha$  and NbAs  $K\beta$  radiation. We find that NbAs (001) stabilizes with a  $45^\circ$  rotational offset with respect to the basal plane (Fig. 3(c)). As stated before, this is due to the lower lattice mismatch in the GaAs  $\langle 110 \rangle$  direction. This agrees with previous reports of TaP and NbP grown on a substrate with cubic crystal structure and high lattice mismatch [14]. The difference in intensity between the peaks at  $0^\circ$  and  $90^\circ$  suggests that there is a preferred direction of alignment of the domains in the sample, probably due to the  $2 \times 4$  GaAs surface reconstruction achieved before the growth. In Fig. 3(d), we see the presence of 3 dominant GaAs peaks with the expected C3 symmetry of GaAs in the (111) direction. We also see the presence of 6 NbAs peaks that are  $60^\circ$  apart. This indicates the presence of domains (twins) that are rotated by  $60^\circ$  with respect to each other. Finally, to understand the structure of the surface of the films, we use atomic force microscopy (AFM) imaging on these samples. In both surfaces (Figs. 3(e) and 3(f)) we see domains that are tens of nanometers in size. The main difference between these different surfaces is that in the (001) plane we see the presence of a rougher surface with domains that show the tetragonal structure of NbAs while in the (100) direction, we have a smoother surface with a higher degree of disorder. This qualitatively agrees with the larger FWHM obtained in the rocking curve in NbAs (100).

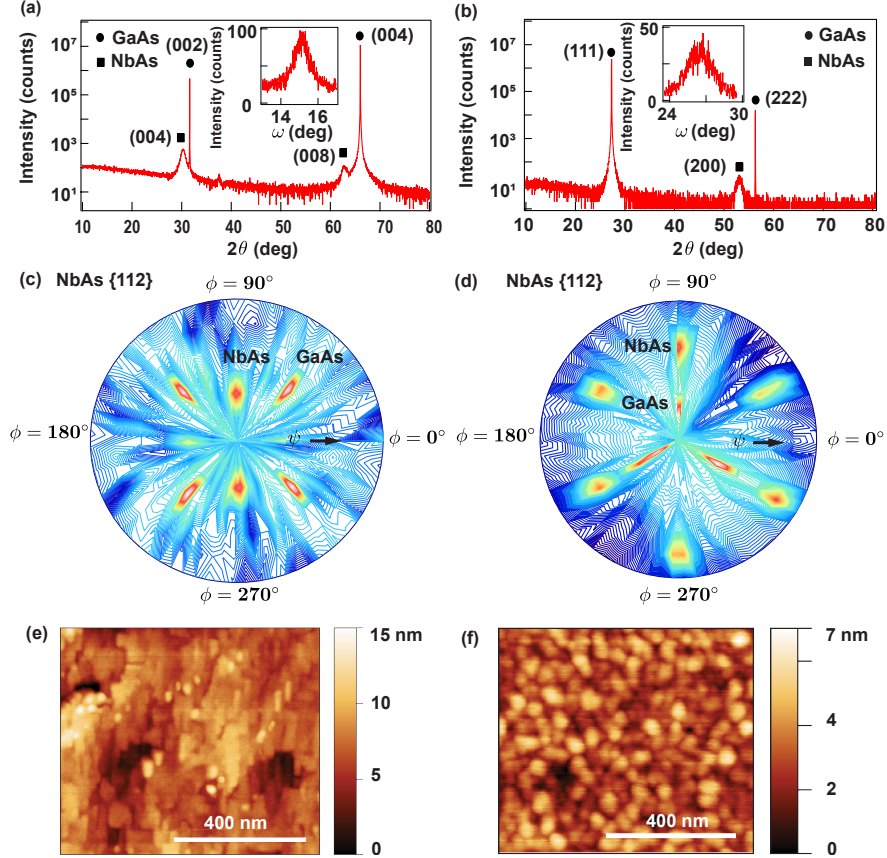


FIG. 3. X-ray diffraction  $2\theta - \omega$  scan of NbAs grown on (a) GaAs (100) and (b) GaAs (111)B. Pole figures around the NbAs  $\{112\}$  direction for samples grown on (c) GaAs (100) and (d) GaAs (111)B. Atomic force microscopy image of (e) NbAs (001) and (f) NbAs (100) showing a root mean square (RMS) surface roughness of 1.4 nm and 0.9 nm respectively.

To understand the microscopic structure of NbAs in the thin film regime, we use HAADF-STEM imaging and energy-dispersive X-ray spectroscopy (STEM-EDX). The results shown in the present manuscript correspond to NbAs (001) grown on GaAs (100). Similar measurements are obtained for NbAs (100)/GaAs (111)B. Figure 4 (a), shows a cross-section HAADF-STEM image of NbAs on GaAs. The NbAs layer is polycrystalline with grain sizes in the range of tens of nanometers, in agreement with the XRD results. The interface between the NbAs and GaAs is diffuse and shows interdiffusion, likely due to the high temperatures required to grow NbAs and the large lattice mismatch with GaAs. The relative concentration of Nb:As and Ga:As is 1:1 in both layers, which confirms the absence of other phases (Fig. 4 (b) and (c)). There is a self-limited oxide layer that covers the top  $\sim 3$  nm of

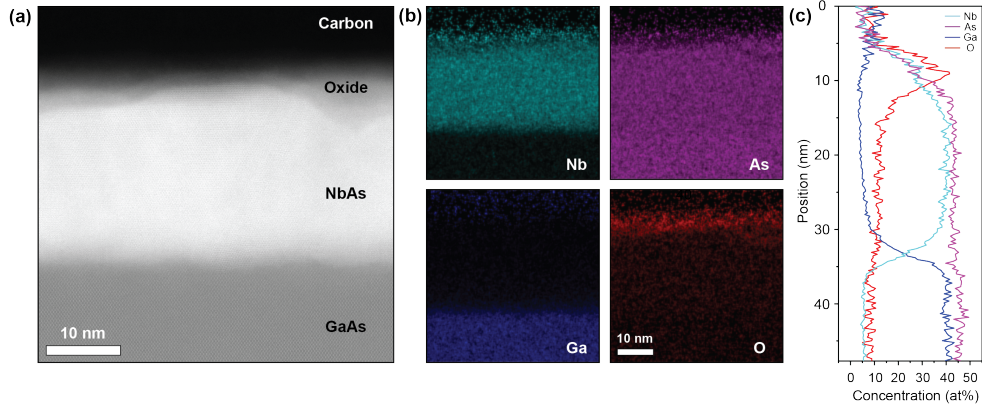


FIG. 4. (a) HAADF-TEM image of the NbAs (001) thin film on a GaAs substrate. (b) STEM-EDX elemental maps of Nb, As, Ga and O in the film. (c) Concentration of the elements in (a) across the NbAs/GaAs interface.

the NbAs film. This is consistent with our previous studies of other topological semimetals such as TaAs and  $\text{Cd}_3\text{As}_2$  [5, 17].

The polycrystalline NbAs layer has domains oriented along the major crystal directions, in addition to the presence of some grain boundaries and twins (Fig. 5(a)). Two such examples are shown in Fig. 5 (b) which are commonly observed in the thin films grown on GaAs. Comparison of the fast Fourier transforms (FFTs) from the grains to the simulated FFTs confirms the two grains to be along the (001) and (100) directions respectively (Fig. 5 (c) and (d)). We note that this is a small subset of several different domains that were identified in NbAs that had more complex orientations that were harder to identify. We believe that more complex microscopy techniques that go beyond the scope of this work (i.e. in plane imaging or statistical analysis of domain orientation) are needed to fully understand the structure of the domains in NbAs thin films.

In order to characterize the electrical properties of the NbAs thin films, we fabricated Hall bars using standard photolithography and Ar plasma etching. The dimensions of the films (length, width and thickness) are  $1000 \mu\text{m} \times 500 \mu\text{m} \times 23 \text{ nm}$  and  $40 \mu\text{m} \times 10 \mu\text{m} \times 10 \text{ nm}$  respectively. Both films show similar qualitative and quantitative behavior. The resistivity ( $\rho$ ) vs. temperature ( $T$ ) in both samples shows activated behavior (Fig. 6(a) and (b)), possibly arising from defects, with  $\rho \approx 450 \mu\Omega \text{ cm}$ . Hall measurements performed at  $T = 2 \text{ K}$  show electrons to be the dominant carrier in both samples (Fig. 6(c) and (d)), with a carrier density ( $n$ )  $6.5 \times 10^{22} \text{ cm}^{-3}$  for NbAs (001) and  $5 \times 10^{21} \text{ cm}^{-3}$  in NbAs

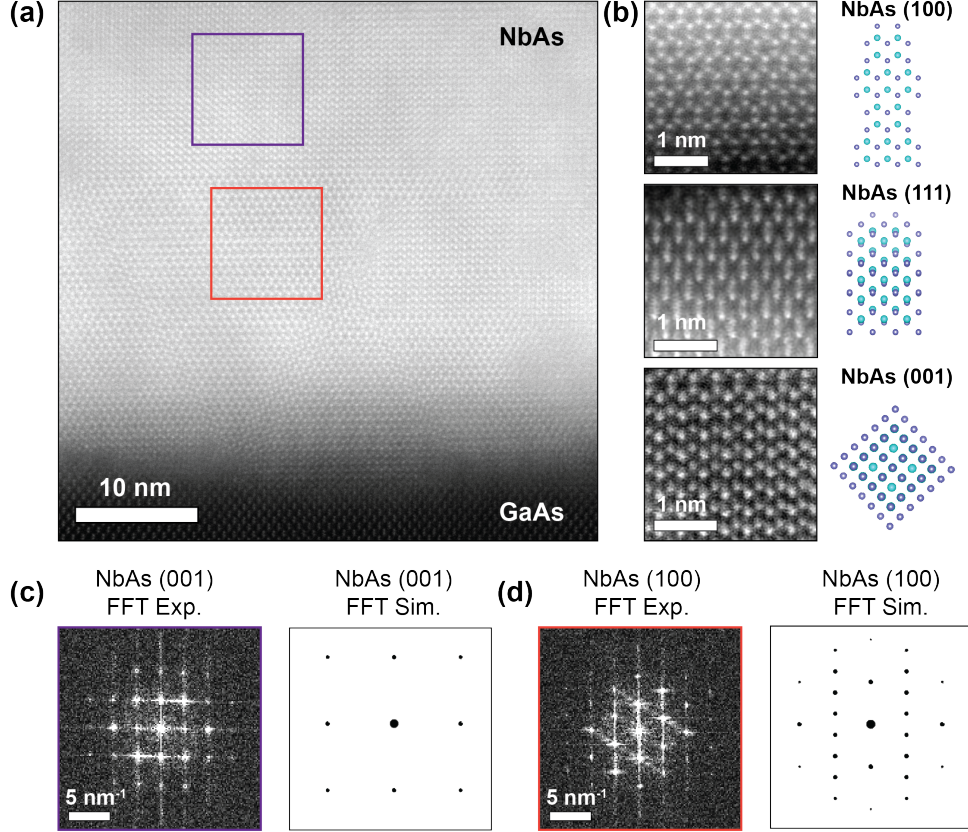


FIG. 5. (a) HAADF-STEM image of NbAs showing polycrystalline structure with multiple grains along different crystal orientations. (b) Common NbAs orientations observed in grains along with the theoretical model. (c) and (d) FFT of the NbAs grains highlighted by the purple and orange boxes respectively along with the simulated FFTs for the (001) and (100) orientations.

(100). The Hall mobility is 0.2 and 2  $\text{cm}^{-2}\text{Vs}$  respectively, while  $k_f l = 2$  and 5 respectively ( $k_f$  is the fermi momentum and  $l$  is the mean free path), implying highly disordered films. Longitudinal resistance measurements at  $T = 2$  K show positive magneto-resistance in both samples (Fig. 6(c) and (d)). Although  $k_f l$  is close to the limit for diffusive transport conditions, as set by the Ioffe-Regel limit ( $k_f l \approx 1$ ), we estimated the phase breaking length ( $l_\phi$ ) in both films using the Hikami-Larkin-Nagaoka expression [18] for weak-antilocalization for high spin-orbit coupled systems:

$$\Delta\sigma = \alpha \frac{e^2}{\pi h} \left[ \psi \left( \frac{1}{2} + \frac{B_\phi}{B} \right) - \ln \left( \frac{B_\phi}{B} \right) \right] \quad (1)$$

Here,  $B_\phi$  is the phase coherence field, and  $\alpha$  is a fitting parameter. We estimate the phase breaking length ( $l_\phi = \sqrt{\frac{\hbar}{4eB_\phi}}$ ) in both films, to be 50 – 80 nm.



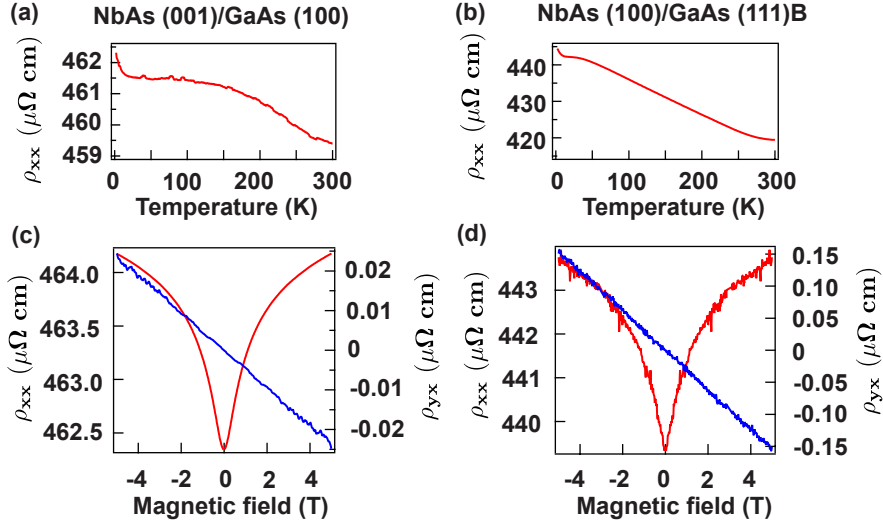


FIG. 6. (a) and (b) Longitudinal resistivity ( $\rho_{xx}$ ) as a function of temperature in 23 nm thick NbAs (001) and 10 nm thick NbAs (100). (c) and (d) Longitudinal resistivity ( $\rho_{xx}$ ) and Hall resistivity ( $\rho_{yx}$ ) as a function of magnetic field in NbAs (001) and (100).

In summary, we report on the synthesis by MBE of Weyl semimetal NbAs thin films on GaAs substrates, a semiconductor of relevance for optoelectronics. We show that different NbAs crystalline orientations can be stabilized by choosing the appropriate substrate orientation. The large lattice mismatch between GaAs and NbAs, coupled with the high growth temperature needed to achieve NbAs growth, induces diffusion at the GaAs/NbAs interface. This hinders the crystallinity of our samples and produces textured films with domains that are tens of nanometers in size. These domains nonetheless have a well defined crystal structure that is oriented in different crystalline directions. Despite the large lattice mismatch, the surface chemistry of GaAs seems to be a decisive factor for effectively nucleating NbAs growth. There is some apparent inconsistency between the textured nature of our films shown in STEM and the clear peaks corresponding to a single crystalline orientation shown in the X-ray diffraction data. We reconcile both measurements by proposing the existence of a preferred crystalline orientation of these domains that can only be seen on a macroscopic scale. More detailed microscopy studies that include statistical analysis and in plane imaging, are required to confirm this hypothesis. We observe that the films naturally oxidize when taken out of vacuum. This effect makes it difficult to access the electronic states of NbAs using surface sensitive techniques like angle resolved photoemission

spectroscopy or scanning tunneling spectroscopy that involve the out-of-vacuum transfer of samples between different vacuum chambers. This suggests caution when trying to probe topological surface states in this family of Weyl semimetals in samples with an oxidized surface. Finally, we expect that further experimental improvements will allow us to increase the degree of crystallinity in NbAs films so that we are able to explore a broader range of physics in this family of well-established Weyl semimetals.

The principal support for this project was provided by SMART, one of seven centers of nCORE, a Semiconductor Research Corporation program, sponsored by the National Institute of Standards and Technology (NIST). This supported the synthesis and standard characterization of NbAs films (WY, YH, NS) and their characterization using STEM (SG, AM). Additional support for materials synthesis and characterization was provided by the Penn State Two-Dimensional Crystal Consortium-Materials Innovation Platform (2DCC-MIP) under NSF Grant No. DMR-2039351 (SI, ES, AR, NS). Parts of this work were carried out in the Characterization Facility, University of Minnesota, which receives partial support from the NSF through the MRSEC (Award Number DMR-2011401) and the NNCI (Award Number ECCS-2025124) programs. SG acknowledges support from a Doctoral Dissertation Fellowship received from the Graduate School at the University of Minnesota. This work utilizes low-temperature transport facilities provided by the Penn State Materials Research Science and Engineering Center under award NSF-DMR 2011839.

---

\* [nsamarth@psu.edu](mailto:nsamarth@psu.edu)

- [1] S.-Y. Xu, I. Belopolski, N. Alidoust, M. Neupane, G. Bian, C. Zhang, R. Sankar, G. Chang, Z. Yuan, C.-C. Lee, S.-M. Huang, H. Zheng, J. Ma, D. S. Sanchez, B. Wang, A. Bansil, F. Chou, P. P. Shibayev, H. Lin, S. Jia, and M. Z. Hasan, Discovery of a Weyl fermion semimetal and topological Fermi arcs, [\*Science\* \*\*349\*\*, 613 \(2015\)](#).
- [2] B. Q. Lv, H. M. Weng, B. B. Fu, X. P. Wang, H. Miao, J. Ma, P. Richard, X. C. Huang, L. X. Zhao, G. F. Chen, Z. Fang, X. Dai, T. Qian, and H. Ding, Experimental discovery of Weyl semimetal TaAs, [\*Phys. Rev. X\* \*\*5\*\*, 031013 \(2015\)](#).
- [3] S.-Y. Xu, I. Belopolski, D. S. Sanchez, M. Neupane, G. Chang, K. Yaji, Z. Yuan, C. Zhang, K. Kuroda, G. Bian, C. Guo, H. Lu, T.-R. Chang, N. Alidoust, H. Zheng, C.-C. Lee, S.-M. Huang, C.-H. Hsu, H.-T. Jeng, A. Bansil, T. Neupert, F. Komori, T. Kondo, S. Shin, H. Lin, S. Jia, and M. Z. Hasan, Spin polarization and texture of the Fermi arcs in the Weyl fermion semimetal TaAs, [\*Phys. Rev. Lett.\* \*\*116\*\*, 096801 \(2016\)](#).
- [4] S.-M. Huang, S.-Y. Xu, I. Belopolski, C.-C. Lee, G. Chang, B. Wang, N. Alidoust, G. Bian, M. Neupane, C. Zhang, S. Jia, A. Bansil, H. Lin, and M. Z. Hasan, A Weyl fermion semimetal with surface Fermi arcs in the transition metal monopnictide TaAs class, [\*Nature Communications\* \*\*6\*\*, 7373 \(2015\)](#).
- [5] W. Yanez, Y. Ou, R. Xiao, S. Ghosh, J. Dwivedi, E. Steinebronn, A. Richardella, K. A. Mkhoyan, and N. Samarth, Giant dampinglike-torque efficiency in naturally oxidized polycrystalline TaAs thin films, [\*Phys. Rev. Appl.\* \*\*18\*\*, 054004 \(2022\)](#).
- [6] X. Yuan, Z. Yan, C. Song, M. Zhang, Z. Li, C. Zhang, Y. Liu, W. Wang, M. Zhao, Z. Lin, T. Xie, J. Ludwig, Y. Jiang, X. Zhang, C. Shang, Z. Ye, J. Wang, F. Chen, Z. Xia, D. Smirnov, X. Chen, Z. Wang, H. Yan, and F. Xiu, Chiral Landau levels in Weyl semimetal NbAs with multiple topological carriers, [\*Nature Communications\* \*\*9\*\*, 1854 \(2018\)](#).
- [7] X. Yuan, C. Zhang, Y. Zhang, Z. Yan, T. Lyu, M. Zhang, Z. Li, C. Song, M. Zhao, P. Leng, M. Ozerov, X. Chen, N. Wang, Y. Shi, H. Yan, and F. Xiu, The discovery of dynamic chiral anomaly in a Weyl semimetal NbAs, [\*Nature Communications\* \*\*11\*\*, 1259 \(2020\)](#).
- [8] D. A. Kealhofer, L. Galletti, T. Schumann, A. Suslov, and S. Stemmer, Topological insulator state and collapse of the quantum Hall effect in a three-dimensional Dirac semimetal

- heterojunction, [Phys. Rev. X \*\*10\*\*, 011050 \(2020\)](#).
- [9] B. J. Ramshaw, K. A. Modic, A. Shekhter, Y. Zhang, E.-A. Kim, P. J. W. Moll, M. D. Bachmann, M. K. Chan, J. B. Betts, F. Balakirev, A. Migliori, N. J. Ghimire, E. D. Bauer, F. Ronning, and R. D. McDonald, Quantum limit transport and destruction of the Weyl nodes in TaAs, [Nature Communications \*\*9\*\*, 2217 \(2018\)](#).
- [10] Y. Sun, Y. Zhang, C. Felser, and B. Yan, Strong intrinsic spin hall effect in the TaAs family of Weyl semimetals, [Phys. Rev. Lett. \*\*117\*\*, 146403 \(2016\)](#).
- [11] S.-Y. Xu, N. Alidoust, I. Belopolski, Z. Yuan, G. Bian, T.-R. Chang, H. Zheng, V. N. Strocov, D. S. Sanchez, G. Chang, C. Zhang, D. Mou, Y. Wu, L. Huang, C.-C. Lee, S.-M. Huang, B. Wang, A. Bansil, H.-T. Jeng, T. Neupert, A. Kaminski, H. Lin, S. Jia, and M. Zahid Hasan, Discovery of a Weyl fermion state with Fermi arcs in niobium arsenide, [Nature Physics \*\*11\*\*, 748 \(2015\)](#).
- [12] I. Vurgaftman, J. R. Meyer, and L. R. Ram-Mohan, Band parameters for III-V compound semiconductors and their alloys, [J. Appl. Phys. \*\*89\*\*, 5815 \(2001\)](#).
- [13] J. Sadowski, J. Z. Domagała, W. Zajkowska, S. Kret, B. Seredyński, M. Gryglas-Borysiewicz, Z. Ogorzałek, R. Bożek, and W. Pacuski, Structural properties of TaAs Weyl semimetal thin films grown by molecular beam epitaxy on GaAs (001) substrates, [Crystal Growth & Design \*\*22\*\*, 6039 \(2022\)](#), <https://doi.org/10.1021/acs.cgd.2c00669>.
- [14] A. Bedoya-Pinto, A. K. Pandeya, D. Liu, H. Deniz, K. Chang, H. Tan, H. Han, J. Jena, I. Kostanovskiy, and S. S. P. Parkin, Realization of epitaxial NbP and TaP Weyl semimetal thin films, [ACS Nano \*\*14\*\*, 4405 \(2020\)](#).
- [15] J. N. Nelson, A. D. Rice, R. Kurlito, A. Shackelford, Z. Sierzega, C.-S. Jiang, A. G. Norman, M. E. Holtz, J. S. Mangum, I. A. Leahy, K. N. Heinselman, H. Ness, M. Van Schilfgaarde, D. S. Dessau, and K. Alberi, [Thin film taas: developing a platform for weyl semimetal devices \(2023\)](#).
- [16] See supplemental material at: [INSERT\\_URL\\_HERE \(2023\)](#).
- [17] W. Yanez, Y. Ou, R. Xiao, J. Koo, J. T. Held, S. Ghosh, J. Rable, T. Pillsbury, E. G. Delgado, K. Yang, J. Chamorro, A. J. Grutter, P. Quarterman, A. Richardella, A. Sengupta, T. McQueen, J. A. Borchers, K. A. Mkhoyan, B. Yan, and N. Samarth, Spin and charge interconversion in Dirac-semimetal thin films, [Phys. Rev. Appl. \*\*16\*\*, 054031 \(2021\)](#).
- [18] S. Hikami, A. I. Larkin, and Y. Nagaoka, Spin-Orbit Interaction and Magnetoresistance in the

Two Dimensional Random System, [Progress of Theoretical Physics](#) **63**, 707 (1980).

- [19] D. MacNeill, G. M. Stiehl, M. H. D. Guimaraes, R. A. Buhrman, J. Park, and D. C. Ralph, Control of spin-orbit torques through crystal symmetry in WTe<sub>2</sub>/ferromagnet bilayers, [Nature Physics](#) **13**, 300 (2017).